03,05

Charge transfer in solid solutions $Bi_{0.9}Sb_{0.1}$ doped with Mn

© A.I. Najafov[1], T.G. Mammadov[1], Kh.V. Aliguliyeva[1,2], S.Sh. Gahramanov[1], V.B. Aliyeva[1], V.N. Zverev[3], N.A. Abdullayev[1,4,¶]

[1] Institute of Physics of the Ministry of Science and Education, Baku, Azerbaijan
[2] Sumgait State University, AZ 5008, Sumgait, Azerbaijan
[3] Institute of Solid State Physics, Russian Academy of Sciences, Chernogolovka, Moscow region, Russia
[4] Baku State University, Baku, Azerbaijan

E-mail: abnadir@mail.ru

Received July 25, 2023
Revised July 25, 2023
Accepted July 26, 2023

Electrical and galvanomagnetic effects in single crystals of $Bi_{0.9}Sb_{0.1}$ solid solutions doped with 1 at.% Mn have been studied. It is shown that in single crystals of $Bi_{0.9}Sb_{0.1}$ solid solutions doped with 1 at.% Mn at temperatures below 180 K, activation conductiity with an activation energy of 10 meV is observed. After thermal annealing, in addition to activation conductivity, at temperatures below 20 K a „metallic" character of conductivity is observed, which is due to conduction over the impurity band. It was found that in single crystals of $Bi_{0.9}Sb_{0.1}$ solid solutions doped with 3 at.% Mn, a „metallic" character of conductivity is observed with a feature at low temperatures of about 25 K, which reacts to applied external magnetic fields. After thermal annealing, the „metallic" nature of the conductivity is retained, but this feature practically disappears. The mobility and concentration of charge carriers are estimated.

Keywords: solid solutions, impurity band, conductivity, magnetoresistance, activation energy.

DOI: 10.61011/PSS.2023.09.57109.164

1. Introduction

From a scientific viewpoint, there are three main reason why the $Bi_{1-x}Sb_x$ solid solutions are of interest: a) depending on the content of Sb atoms, these compounds are metals, semiconductors or semimetals; b) the $Bi_{1-x}Sb_x$ solid solutions are used as materials for high-performance thermoelectric transducers; c) $Bi_{1-x}Sb_x$ are topological insulators.

It has been found that with increasing content of Sb atoms in the $Bi_{1-x}Sb_x$ solid solution, overlap between the conduction band L_s and valence band T decreases and a gapless state is observed at $0 \le x < 0.04$ [1,2]. With further growth of x, bands L_a and L_s are inverted, and at $x \sim 0.07$ overlap between the conduction band and valence band is equal to zero and the material loses its semimetallic properties becoming a semiconductor [3,4].

In the Sb atom concentration range $0.07 < x < 0.22$, the alloys are semiconductors characterized by small energy gap whose maximum values is within 16–17 at.% Sb [5,6].

With further increase in the content of Sb atoms, the energy gap decreases again, and at $x \sim 0.22$ the $Bi_{1-x}Sb_x$ compound changes into the gapless state again, and at $x > 0.22$ becomes a semimetal [7,8] (Figure 1, *a*).

Experimental data on the temperature dependence of resistance within 4.2–300 K are reported in [9]. It is shown how energy gaps determined from the activation energy vary in the $Bi_{1-x}Sb_x$ solid solutions depending on x (Figure 1, *b*). The Figure shows that the maximum energy gap of 14 meV is achieved at the Sb atom concentrations about 12–13%. In [5], the similar investigations demonstrate that the maximum energy gap about 20 meV is achieved at the Sb atom concentrations about 15–16%.

As mentioned above, the $Bi_{1-x}Sb_x$ compounds are high-performance thermoelectric materials. In [10,11], it is shown that the highest thermoelectric performance $Z_{max} = 5 \cdot 10^{-3}\,K^{-1}$ is achieved for the composition with $x = 0.12$ at 80 K. At 300 K, thermoelectric performance in this compound decreases to $1 \cdot 10^{-3}\,K^{-1}$. It is pointed out that $Z_{max} = 1.8 \cdot 10^{-3}\,K^{-1}$ at room temperature is observed for the compound with $x = 0.05$.

The Table contains the maximum thermoelectric performance data Z_{max} for the $Bi_{0.95}Sb_{0.05}$ compound and other thermoelectric materials at room temperature.

Current research shows that considerable increase in thermoelectric performance can be achieved by using low-dimensional structures based on the $Bi_{1-x}Sb_x$ solid solutions. Recently [14–16] have shown that the thermoelectric performance of the $Bi_{1-x}Sb_x$ solid solutions may be increased by producing structures consisting of micron-size grains in [17].

It is reported that inclusion of Bi nanotubes in $Bi_{1-x}Sb_x$ alloy at $x = 0.15$ results in significant thermal conductivity decrease and considerable increase of absolute Seebeck

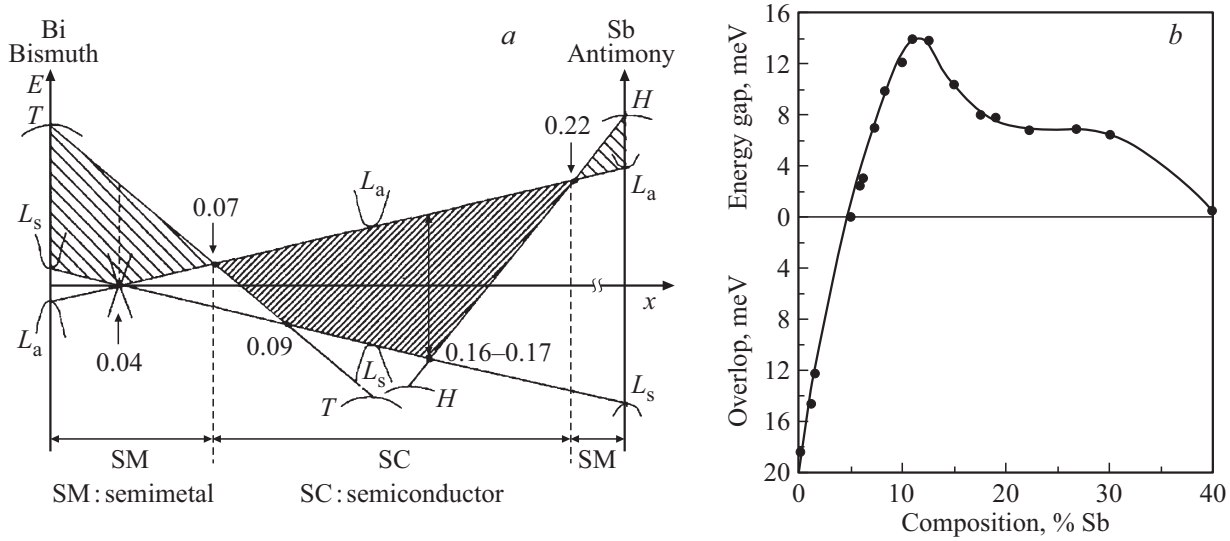

Figure 1. *a*) Energy band variations near the Fermi level in the $Bi_{1-x}Sb_x$ solid solutions depending on the content of Sb atoms [5]; *b*) energy gap in the $Bi_{1-x}Sb_x$ solid solutions depending on the content of Sb atoms [9].

Maximum thermoelectric performance Z_{max} of some semiconductor compound at room temperature

Semiconductor	Z_{max} $(10^{-3}\,K^{-1})$	Reference
$Bi_{0.95}Sb_{0.05}$	1.8	[10,11]
Bi_2Te_3	2	[10,11]
$AgSbTe_2$	1.2	[12]
PbTe	1.2	[13]
InSb	0.47	[13]
GeSi	0.9	[13]

coefficients leading to increased ZT up to 0.3. In [18] it has been found that substitution of Bi atom by Sb atom in $Bi_{1-x}Sb_x$ monolayers considerably reduces the lattice and electronic thermal conductivity and electrical conductivity that in total results in the increase of the thermoelectric performance up to 0.81.

The interest in the $Bi_{1-x}Sb_x$ solid solutions cover a wide range of applications and has increased recently due to the discovery of new applications for these materials. Primarily, the studies shall be noted which are devoted to applications of spin-directed currents typical for surface states in spintronics and in information transfer, writing and storage media [19,20], in high THz radiation devices [21] and as high-performance cathode materials for water zinc cells [22].

Since 2007 the $Bi_{1-x}Sb_x$ solid solutions and several other structures (α-Sn and HgTe) have been classified as a new group of crystals — topological insulators [23]. As shown in Figure 1, *a*, at Sb concentration of 4%, bands L_a and L_s intersect forming the Dirac points (point where the conduction bands and valence band intersect). Further increase in Sb concentration results in inversion of bands L_a and L_s, and at $x = 0.07$, the valence band energy T becomes lower than that of the conduction band L_a — $Bi_{1-x}Sb_x$ becomes a semiconductor with indirect band gap (Figure 1, *a*) [5,24]. At Sb concentrations from 7 to 22%, the bands do not intersect anymore, and $Bi_{1-x}Sb_x$ becomes a topological insulator with inverted band [25–27].

When magnetic impurities are introduced in the topological insulator by doping, exotic physical phenomena may be observed on the surface such as quantized abnormal Hall (QAH), axion electrodynamics, magnetoelectric effect, Majorana fermions, etc. [29–31] due breaking of symmetry with respect to time sign reversal or calibration symmetry [28]. Taking into account the unique properties of surface states in the electronic spectra of topological insulators, there has been recently an increasing number of studies devoted to production and investigation of low-dimensional thin-film structures of the $Bi_{1-x}Sb_x$ solid solutions applied or grown on various substrates [32–35].

Investigations of the effect of magnetic Mn impurities on the electrical and galvanomagnetic properties of the $Bi_{0.9}Sb_{0.1}$ solid solution are reported herein. It should be noted that by the time of writing this paper, no studies in this field had been reported in the literature. Only the recent paper [16] reports the studies of electrical conductivity in a limited temperature range 80−300 K.

The main objective of this research is to detect the influence of magnetic spin ordering of Mn atoms on charge transfer in Mn-doped $Bi_{0.9}Sb_{0.1}$ in the low temperature region.

2. Preparation and characterization of the prepared Mn-doped $Bi_{0.9}Sb_{0.1}$ solid solution samples

It is known [36] that a continuous series of $Bi_{1-x}Sb_x$ solid solutions is formed in the phase diagram of the Bi-Sb

system. This is caused by the isostructurality of the Bi and Sb lattices with the difference in their atomic sizes of only 7%. Solubility of Mn in the $Bi_{1-x}Sb_x$ solid solutions has been investigated in detail, however, as shown by the Bi-Mn, Sb-Mn and Bi-Sb-Mn phase diagrams [37], it is not high. Therefore, to study the solubility and the effect of Mn impurities on the electrical and galvanomagnetic properties of the $Bi_{1-x}Sb_x$ solid solutions, $Bi_{0.9}Sb_{0.1}$ compounds with low Mn concentrations of 1.0 and 3.0 at.% were prepared. $Bi_{1-x}Sb_x$: Mn (1.0; 3.0 at.%) alloys were synthesized in extra-pure argon atmosphere by the ampoule technique. The $Bi_{1-x}Sb_x$ solid solutions were synthesized from the initial 99.999% purity Bi, Sb and Mn taken in stoichiometric ratios. The synthesis process was carried out at 700°C by melting and holding at this melt temperature for 4 hours.

The $Bi_{1-x}Sb_x$: Mn (1.0; 3.0 at.%) solid solution crystals were grown by the directional solidification method at 400°C. The ampoule movement rate was 0.2 mm per hour. As a result, single-crystal ingots 40 mm in size and 8.0 mm in diameter were produced and used to chip off 5 to 6 appropriate measurement samples.

X-ray diffraction data were obtained using „D2 Phaser" diffractometer, and phase analyses were carried out by the Rietveld method using standard EVA and TOPAS-4.2 software (Bruker, Germany).

X-ray diffraction reflections typical for $Bi_{0.9}Sb_{0.1}$ single-crystals were recorded within $5° \le 2\theta \le 80°$ [38,39] (Figure 2). The obtained Mn-doped $Bi_{0.9}Sb_{0.1}$ single-crystals have space group R-3m with lattice parameters $a = 4.5325(2)$, $c = 11.8345(5)$. Note that doping with magnetic Mn impurities in such minor concentrations (1–3%) does not result in significant changes in the angular X-ray reflection positions.

Raman scattering in Mn-doped $Bi_{0.9}Sb_{0.1}$ was examined using „Nanofinder 30" (Tokyo Instr., Japan) Raman microspectrometer. The investigations were carried out in backscattering geometry. The second harmonic of $\lambda = 532$ nm YAG:Nd laser was used as the excitation light source. A cooled (−70°C) CCD camera operating in the photon counting mode served as a radiation receiver. The exposure time was generally 3 min., maximum incident radiation power on the sample was 10 mW, beam diameter was 4 μm. The spectrometer used a 1800 g/mm diffraction grating, the spectral line position measurement accuracy was 0.5 cm^{-1} or better. The Raman scattering spectra in the Mn-doped $Bi_{0.9}Sb_{0.1}$ single-crystals are shown in Figure 3.

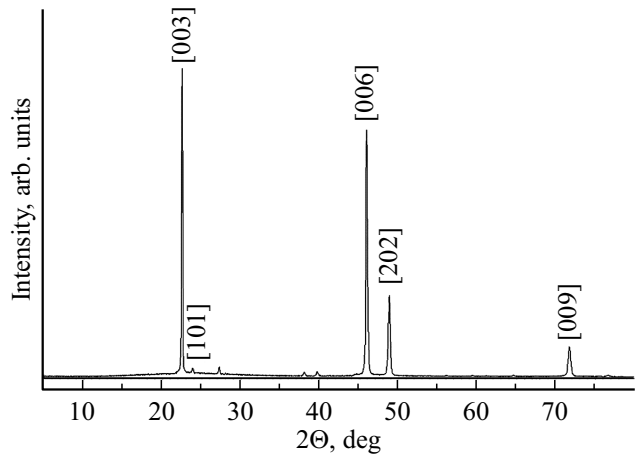

Figure 2. X-ray diffraction of the Mn-doped (3%)$Bi_{0.9}Sb_{0.1}$ solid solution single-crystals.

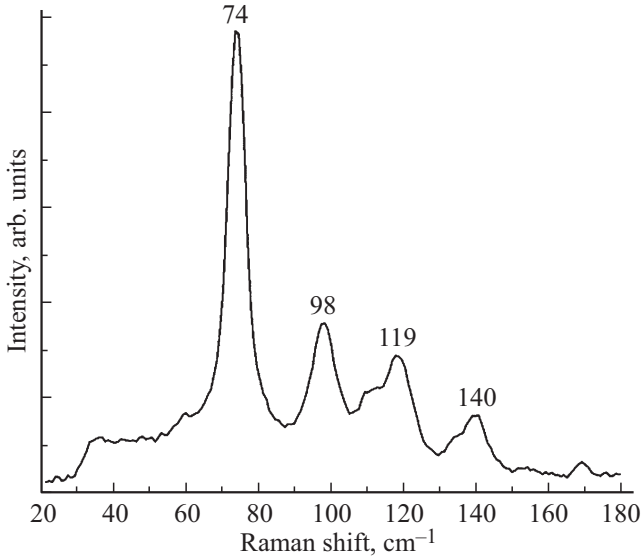

Figure 3. Raman light scattering of the Mn-doped (3%)$Bi_{0.9}Sb_{0.1}$ solid solution single-crystals.

As shown in Figure 3, in the $Bi_{0.9}Sb_{0.1}$ crystals doped with Mn 3%, RS-active phonons with 74, 98, 119 and 140 cm^{-1} frequencies are observed. This results agrees closely with the findings of [38] obtained on undoped samples.

3. Electrical and galvanomagnetic effects in the Mn-doped $Bi_{0.9}Sb_{0.1}$ solid solutions

Electrical and galvanomagnetic (Hall effect and magnetoresistance) effects in the Mn-doped $Bi_{0.9}Sb_{0.1}$ single-crystals were studied by the standard four-probe method with selective technique at 20.5 Hz AC using Lock-in Amplifier-SR830. The current was maximum 1 mA. The investigations were carried out in a wide temperature range 5–300 K. Strong magnetic fields up to 80 kOe were achieved using a superconducting solenoid. For galvanomagnetic measurements, the sample was placed in center of the solenoid.

Figure 4 shows the resistivity vs. temperature curves for the $\rho(T)$ $Bi_{0.9}Sb_{0.1}$ doped with 1 at.% Mn.

As shown in Figure 4, *a*, a normal „semiconductor" behavior of the resistivity ρ vs. temperature curve is observed: with temperature decrease at high temperatures ($T < 300$ K), resistivity decreases due to increasing charge carrier mobility, and at lower temperatures ($T < 180$ K)

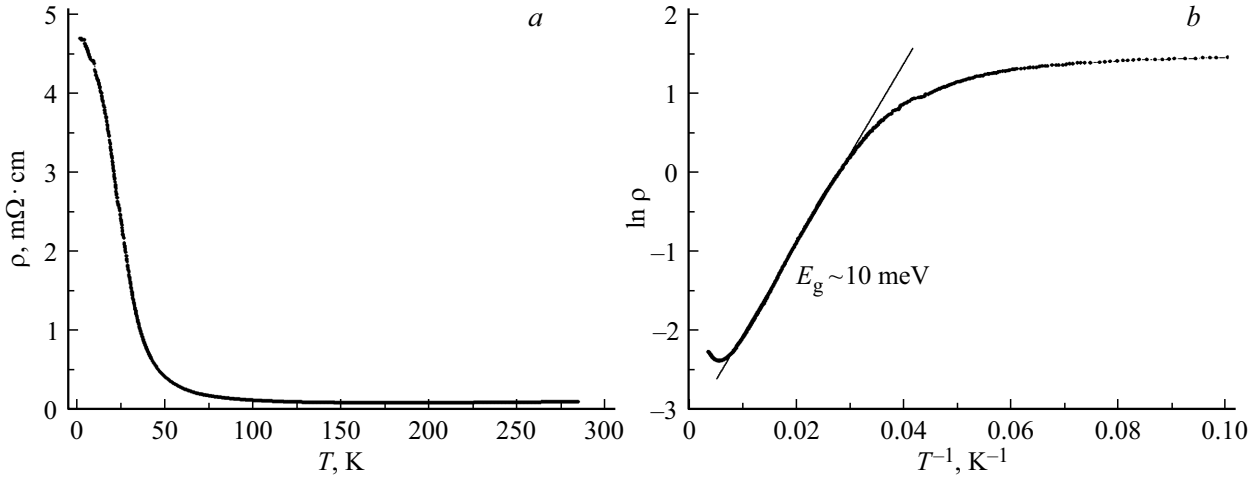

Figure 4. Temperature vs. resistivity — $Bi_{0.9}Sb_{0.1}$ doped with 1 at.% Mn: *a*) in coordinates $\rho(T)$; *b*) in the Arrhenius coordinates.

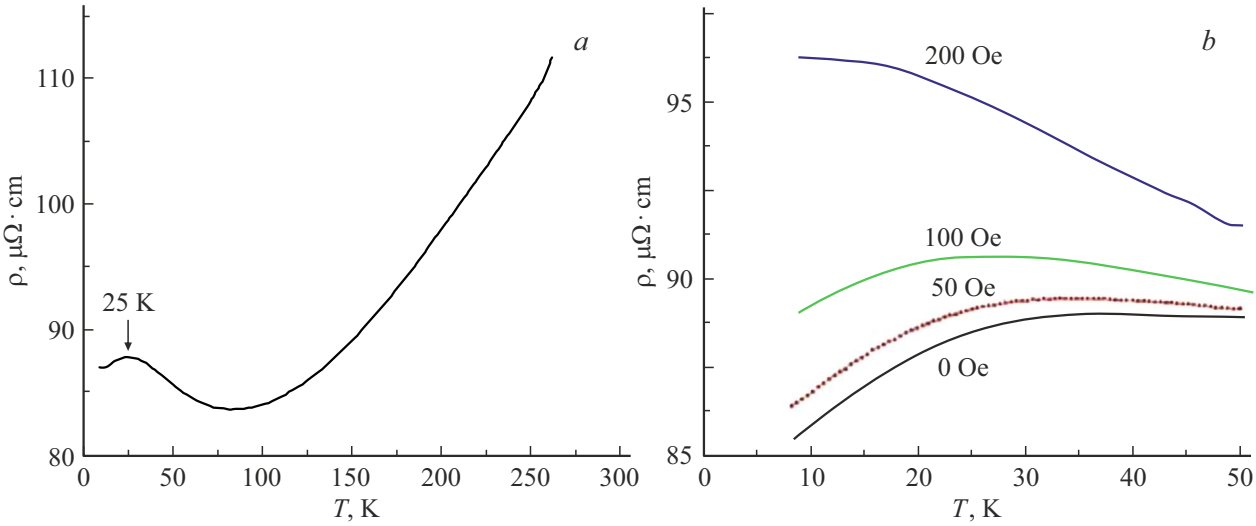

Figure 5. temperature vs. resistivity for $Bi_{0.9}Sb_{0.1}$, doped with 3 at.% Mn: *a*) without magnetic field; *b*) under applied external magnetic fields $H = 0$, 50, 100 and 200 Oe.

with further temperature decrease, exponential resistivity growth is observed due to the decreasing charge carrier concentration. The activation energy determined from $\ln\rho(T^{-1})$ in the Arrhenius coordinates (Figure 4, *b*) was equal to $\Delta E = 10$ meV that agrees closely with the data in [9] for $Bi_{0.9}Sb_{0.1}$ (Figure 1, *b*).

According to the Hall measurements, the charge carrier concentration at room temperature $T = 300$ K for all samples (doped with 1 and 3 at.% Mn) varied within $7.4 \cdot 10^{17} - 2 \cdot 10^{18}$ cm^{-3}. With temperature decrease to 5 K, the 1 at.% Mn-doped samples had activation conductivity and the charge carrier concentration decreased considerably to $(2.6-3.3) \cdot 10^{16}$ cm^{-3}. For the sample shown in Figure 4, the charge carrier concentration was about $1.5 \cdot 10^{18}$ cm^{-3}, thus, the mobility was $3.8 \cdot 10^4$ cm^2/V · s, and at $T = 5$ K, the concentration decreased considerably — $2.6 \cdot 10^{16}$ cm^{-3} with the mobility equal to $5.1 \cdot 10^4$ cm^2/V · s.

Of special interest are the investigations of temperature dependences of resistivity for the $Bi_{0.9}Sb_{0.1}$ solid solution doped with 3 at.% Mn (Figure 5). It should be primarily noted that „metallic“ conductivity behavior is observed throughout the temperature range 5–300 K — the resistivity decreases with decreasing temperature. High Mn atom doping concentrations probably result in considerable amount of defects (antisite and intersite) inducing numerous energy levels in the band gap that form a wide impurity band that completely covers the band gap. This phenomenon is typical for narrow-band semiconductors, e.g. Bi_2Te_3, where the „metallic“ type of conductivity is observed initially due to a lot of antisite defects ($10^{18}-10^{19}$ cm^{-3}) [40].

With the temperature decrease from 300 K to 80 K, the resistivity decreases and increases with further temperature decrease and achieves its maximum at $T = 25$ K (Figure 5, *a*). Such feature in the temperature dependence

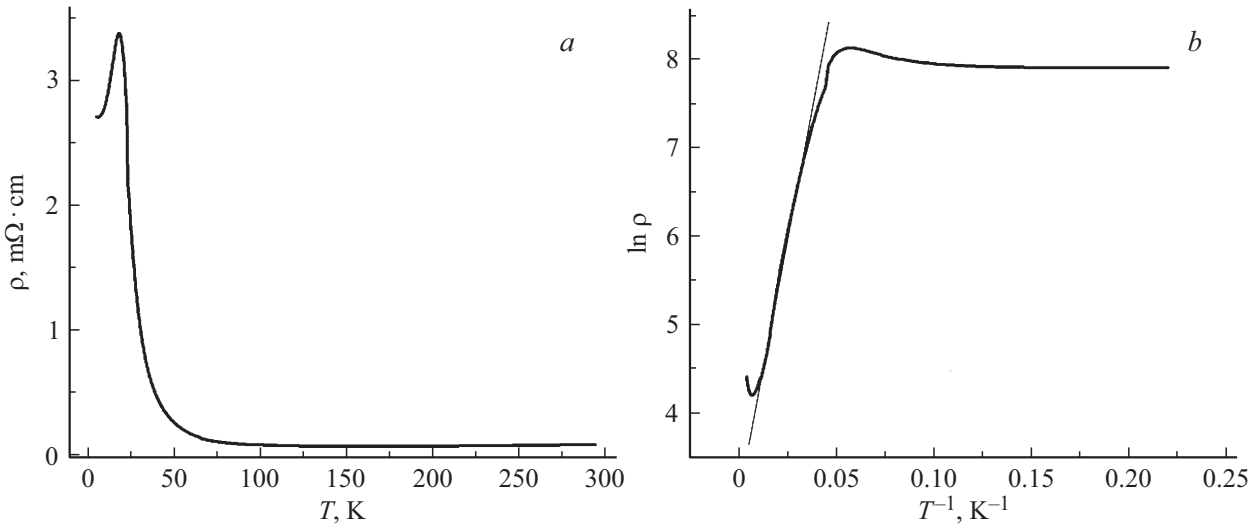

Figure 6. Temperature vs. resistivity curves for the $Bi_{0.9}Sb_{0.1}$ samples doped with 1 at.% Mn after annealing.

of the resistivity of $Bi_{0.9}Sb_{0.1}$ doped with 3 at.% Mn is probably attributable to spin fluctuations occurring during the magnetic phase transition in magnetic topological insulators [41,42]. To find the nature of this feature in $\rho(T)$, the influence of external magnetic fields on the temperature dependence $\rho(T)$ was studied. Figure 5, *b* shows that the feature on $\rho(T)$ responds to weak external magnetic fields and almost disappears when the external magnetic field is 200 Oe. Disappearance of the feature on $\rho(T)$ in weak magnetic fields 200 Oe confirms weak magnetic ordering of magnetic Mn atom spins.

Thermal annealing of the samples was carried out to order the magnetic Mn atoms in the crystal lattice of the test compounds. Annealing was carried out at $T = 220^{\circ}$C in vacuum during 600 h. It should be noted that after thermal annealing no significant changes were found either in X-ray diffraction patterns or Raman scattering spectra. Figure 6 shows the temperature vs. resistivity curves for the annealed $Bi_{0.9}Sb_{0.1}$ samples doped with 1 at.% Mn.

After annealing, the activation energy estimated from Figure 6, *b* was almost unchanged: $\Delta E = 9.5$ meV, however, the low-temperature portion of $\rho(T)$ changed considerably. After low-temperature exponential growth of ρ, $\rho(T)$ demonstrates the „metallic" behavior with decreasing temperature below 20 K. It should be noted that this feature on $\rho(T)$ does not respond to the applied external magnetic fields.

The metal–insulator transition is experimentally observed in many materials [43], but the samples studied herein showed an unusual „metallic" behavior of conductivity during the metal–insulator transition at low temperatures and „insulating" or activation behavior — at higher temperatures. Similar cases of „unusual" temperature behavior of electrical cinductivity are known in the literature [43–49]. Low radius polarons behave at low temperatures similarly to a free particle with increased weight, and at high temperatures ($kT > h\nu/2$ (ν — phonon frequency) they move with thermally activated jumps [42]. Since the addressed objects are nonpolar substances, this version may be rejected.

It is suggested in [46–48] that the conductivity in a lamellar crystal takes place perpendicularly to the layers via two parallel channels — „metallic" and „activation" channels. This model assumes that charge transfer takes place via competing narrow conducting filamentary paths and wide disordering regions through phonon-induced jumps of the charge carriers over the localized states. At low temperatures, conductivity via narrow „metallic" channels prevails. However, the effects observed in these studies occurs at relatively high temperatures — $T \approx 150$ K. It has been demonstrated in [49] that for weakly disordered systems such as doped solid solutions, a quantum interference phenomenon — slight antilocalization may be observed at low temperatures (usually below 5–10 K), when the resistance decreases with temperature decrease. However, in this case, when the external magnetic field is applied, positive magnetoresistance with typical field dependence shall be observed.

In [44,45] it has been shown that a hump similar to that on Figure 6, *a* is observed at 25–30 K on $\rho(T)$ in the Sb-doped Ge crystals. The „metallic" type of conductivity is attributable to the presence of a narrow impurity band. At high temperatures, conductivity in the conduction band with high electron mobility play the leading role, then activation conductivity is observed due to the exponential decrease in the electron concentration until the band conductivity becomes equal to the impurity conductivity, and the conductivity in the impurity band is prevailing at low temperatures. It should be noted that the previous studies of the $Bi_{1-x}Sb_x$ solid solutions also identified the presence of humps on $\rho(T)$ [5]. The hump peak position depends on the Sb atom content and varies from 30 K to 50 K. The low-temperature „metallic" conductivity is also explained by the presence of the impurity band. This may be qualitatively

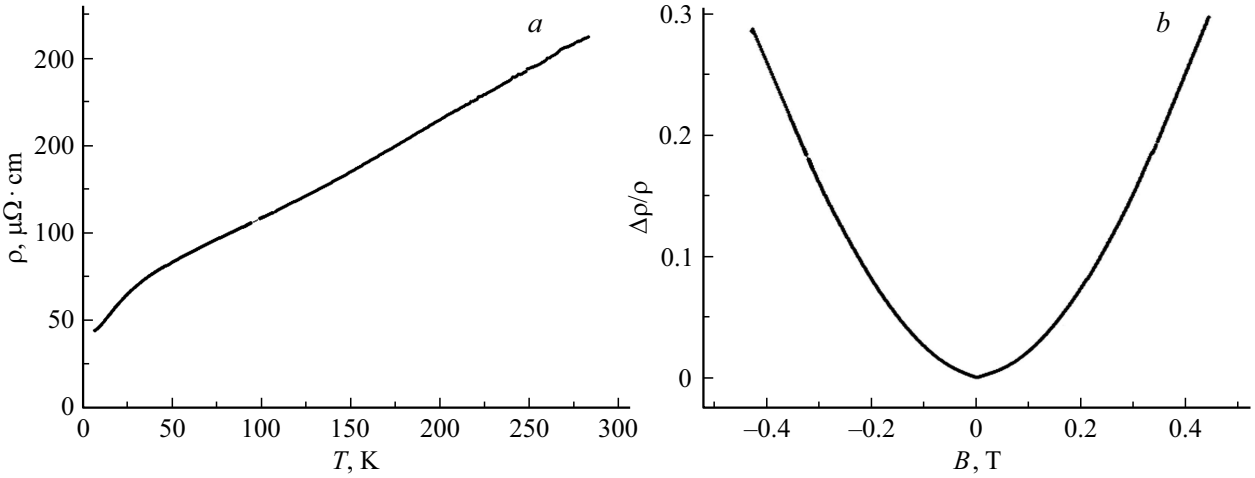

Figure 7. $Bi_{0.9}Sb_{0.1}$ solid solution doped with 3 at.% Mn after thermal annealing: *a*) temperature vs. resistivity $\rho(T)$; *b*) field vs. transverse magnetoresistance $(\Delta\rho/\rho)$ at $T = 5$ K.

understood using the ionization energy E_i (1) and Bohr radius a_B (2) expressions for the bound electron near the impurity ion [5]:

$$E_i(\text{eV}) = 13.6 \cdot \left(\frac{m^*}{m_0}\right) \frac{1}{\varepsilon_r^2}, \tag{1}$$

$$a_B(\text{cm}) = 0.53 \cdot \left(\frac{m_0}{m^*}\right) \cdot \varepsilon_r \cdot 10^{-8}. \tag{2}$$

Taking into account the effective electron mass $m^* = 0.01m_0$ according to the cyclotron resonance experiments and high dielectric constant $\varepsilon_r = 100$ [50] in these crystals, low ionization energy $E_i = 10^{-5}$ eV and large Bohr radius $a_B = 530$ nm are obtained. Such large Bohr radius results in formation of an impurity band even at low impurity concentrations n_i. The heavy doping condition $a_B^3 n_i \gg 1$ [51] is satisfied at sufficiently low impurity concentrations $10^{13}-10^{14}$ cm^{-3}. Therefore, the impurity band overlap the conduction band and the conductivity at low temperatures is „metallic“ in nature.

Resistivity vs. temperature for the $Bi_{0.9}Sb_{0.1}$ solid solution doped with 3at.% Mn after thermal annealing are shown in Figure 7, *a*. As shown in Figure 7, *a*, $\rho(T)$ after thermal annealing demonstrates the „metallic“ behavior throughout the studied temperature range, however, the hump-type feature (Figure 5, *a*) disappears — only a knee remains at $T = 25$ K.

The thermal annealing, contrary to the expectations, probably causes even higher disordering in the magnetic atom arrangement.

Figure 7, *b* shows the transverse magnetoresistance vs. magnetic field $(\Delta\rho/\rho)$ at $T = 5$ K for thermally annealed $Bi_{0.9}Sb_{0.1}$ solid solution samples doped with 3 at.% Mn. As shown in Figure 7,*b*, the magnetoresistance is high and increasing in resistivity by 25% $(\Delta\rho/\rho = 0.25)$ is observed in the magnetic field $B = 0.4$ T suggesting high mobility of the charge carriers. Figure 7, *b* also clearly shows the typical Lorentz quadratic dependence of the magnetoresistance on the magnetic field B:

$$\Delta\rho/\rho = \mu^2 B^2, \tag{3}$$

here μ is the charge carrier mobility.

Mobility μ estimated from (3) was approximately equal to $1.5 \cdot 10^4$ cm^2/V · s at $T = 5$ K. The similar quantity is obtained for μ also from

$$\sigma = en\mu = 1/\rho, \tag{4}$$

here n is the charge carrier concentration.

The Hall experiments determined that the concentration for this sample $n = 7.4 \cdot 10^{17}$ cm^{-3}.

4. Conclusion

Thus, the $Bi_{0.9}Sb_{0.1}$ solid solution single-crystals doped with 1 at.% and 3 at.% magnetic Mn atoms have been obtained herein. The X-ray diffraction and Raman scattering data agree closely with the reported data for the undoped $Bi_{0.9}Sb_{0.1}$ solid solutions. An activation-type conductivity with an activation energy of 10 meV has been found in the $Bi_{0.9}Sb_{0.1}$ solid solution doped with 1 at.% Mn. The novelty of the findings is in that the „metallic“ type conductivity is observed on $\rho(T)$ throughout the studied temperature range 5–300 K with a hump-type feature at 25 K in the $Bi_{0.9}Sb_{0.1}$ solid solution doped with 3 at.% Mn. Response of this feature to the applied external magnetic fields confirms its magnetic nature. It is shown that the hump on $\rho(T)$ disappears at the external magnetic field of $H = 200$ Oe.

After thermal annealing of the same samples, considerable changes take place in $\rho(T)$. In the $Bi_{0.9}Sb_{0.1}$ solid solution doped with 1 at.% Mn, the activation behavior of conductivity at temperatures below 100 K is maintained with the activation energy of 9.5 meV, however, at lower temperatures (below 20 K), $\rho(T)$ changes to the „metallic“

type of conductivity. This is attributable to the presence of the impurity band. Due to low effective weight of the charge carriers ($m^* = 0.01m_e$) and high dielectric constant ($\varepsilon_r = 100$), the Bohr radius of the bound electron near the impurity ion increases considerably up to 530 nm. Therefore, the heavy doping condition $a_B^3 n_i \gg 1$ is satisfied at sufficiently low impurity concentrations. Thus, the impurity band occurs and overlaps the conduction band, and the conductivity at low temperatures is „metallic" in nature. After thermal annealing, $\rho(T)$ in the $Bi_{0.9}Sb_{0.1}$ solid solution doped with 3 at.% Mn still demonstrates the „metallic" behavior throughout the studied temperature range, however, the hump-type feature disappears and only a knee remains at $T = 25$ K. The thermal annealing probably facilitates disordering in the magnetic atom arrangement.

Funding

This study was financially supported by the Foundation for the Development of Science under the President of the Republic of Azerbaijan (grants No. EİF/MQM/Elm-Tehsil-1-2016-1(26)-71/16/1 and № EİF-BGM-3-BRFTF-2^+/2017-15/02/1).

Conflict of interest

The authors declare that they have no conflict of interest.

References

[1] E.J. Tichovoisky, J.G. Mavroides. Solid State Commun. **7**, *13*, 927 (1969).
[2] G. Oelgart, R. Herrmann. Phys. Status Solidi B **75**, *1*, 189 (1976).
[3] M.R. Ellett, R.B. Horst, L.R. Williams, K.F. Cuff. Proc. Int. Conf. Phys. Semiconductors. Kyoto (1966). J. Phys. Soc. Jpn. 21 Suppl. 666 (1966).
[4] P.W. Chao, H.T. Chu, Y.H. Kao. Phys. Rev. B **9**, *10*, 4030 (1974).
[5] B. Lenoir, M. Cassart, J.-P. Michenaud, H. Scherrer, S. Scherrer. J. Phys. Chem. Solids **57**, *I*, 89 (1996).
[6] B. Lenoir, H. Scherrer, T. Caillat. Semicond. Semimet. **69**, 101 (2001).
[7] G. Oelgart, G. Schneider, W. Kraak, R. Herrmann. Phys. Status Solidi B **74**, *1*, K75 (1976).
[8] W. Kraak, G. Oelgart, G. Schneider, R. Herrmann. Phys. Status Solidi B **88**, *1*, 105 (1978).
[9] A.L. Jain. Phys. Rev. **114**, *6*, 1518 (1959).
[10] G.E. Smith, R. Wolfe. J. Appl. Phys. **33**, *3*, 841 (1962).
[11] A.M. Ibrahim, D.A. Thomson. Mater. Chem. Phys. **12**, *1*, 29 (1985).
[12] F.D. Rosi. Solid-State Electronics **11**, *9*, 833 (1968).
[13] D.A. Wright. Metallurg. Rev. **15**, *1*, 147 (1970).
[14] Sh. Gao, J. Gaskins, X. Hu, K. Tomko, P. Hopkins, S.J. Poon. Sci. Rep. **9**, 14892 (2019).
[15] M.N. Norizan, Y. Ohishi, K. Kurosaki, H. Muta. Mater. Transact. **60**, *6*, 1072 (2019).
[16] A.M. Ahmed, H.F. Mohamed, A.K. Diab, E.Y. Omar. Inf. Sci. Lett. **12**, *1*, 149 (2023).
[17] E. Gunes, B. Landschreiber, D. Hartung, M.T. Elm, C. Rohner, P.J. Klar, S. Schlecht. J. Elektron. Mater. **43**, *6*, 2127 (2014).
[18] C.Y. Wu, J. Han, L. Sun, H. Gong. J. Mater. Chem. C **8**, *2*, 581 (2020).
[19] Z. Chi, Y.-Ch. Lau, X. Xu, T. Ohkubo, K. Hono, M. Hayashi. Sci. Adv. **6**, *10*, 2324 (2020).
[20] E. Rongione, L. Baringthon, D. She, G. Patriarche, R. Lebrun, A. Lemaitre, M. Morassi, N. Reyren, M. Micica, J. Mangeney, J. Tignon, F. Bertran, S. Dhillon, P. Le Fevre, H. Jaffres, J.-M. George. Adv. Sci. Early View 2301124 (2023).
[21] S. Rho, H. Park, J. Park, K. Jeong, H. Kim, S.-B. Hong, J. Kim, H.W. Lim, Y. Yi, Ch. Kang, M.-H. Cho. Adv. Funct. Mater. Early View 2300175 (2023).
[22] Zhao, F. Jiang, H. Hong, D. Wang, Q. Li, Y. Meng, Z. Huang, Y. Guo, X. Li, A. Chen, R. Zhang, Sh. Zhang, J.C. Ho, Z. Yao, W. Liu, Ch. Zhi. Mater. Today **51**, 87 (2021).
[23] L. Fu, C.L. Kane, E.J. Mele. Phys. Rev. Lett. **98**, *10*, 106803 (2007).
[24] L. Fu, C.L. Kane. Phys. Rev. B **76**, *4*, 045302 (2007).
[25] J.C.Y. Teo, L. Fu, C.L. Kane. Phys. Rev. B **78**, *4*, 045426 (2008).
[26] A.A. Taskin, Y. Ando. Phys. Rev. B **80**, *8*, 085303 (2009).
[27] D. Hsieh, Y. Xia, L. Wray, D. Qian, A. Pal, J.H. Dil, J. Osterwalder, F. Meier, G. Bihlmayer, C.L. Kane, Y.S. Hor, R.J. Cava, M.Z. Hasan. Science **323**, *5916*, 919 (2009).
[28] Y.L. Chen, J.-H. Chu, J.G. Analytis, Z.K. Liu, K. Igarashi, H.-H. Kuo, X.L. Qu, S.K. Mo, R.G. Moore, D.H. Lu, M. Hashimoto, T. Sasagawa, S.C. Zhang, I.R. Fisher, Z. Hussain, Z.X. Shen. Science **329**, *5992*, 659 (2010).
[29] J. Maciejko, X.L. Qi, H.D. Drew, S.C. Zhang. Phys. Rev. Lett., **105**, *16*, 166803 (2010).
[30] W.-K. Tse, A.H. MacDonald. Phys. Rev. B **82**, *16*, 161104 (2010).
[31] W.-K. Tse, A.H. MacDonald. Phys. Rev. Lett. **105**, *5*, 057401 (2010).
[32] T. Fan, M. Tobah, T. Shirokura, N.H.D. Khang, P.N. Hai. Jpn. J. Appl. Phys. **59**, *6*, 063001 (2020).
[33] L. Aggarwal, P. Zhu, T.L. Hughes, V. Madhavan. Nature Commun. **12**, *1*, 4420 (2021).
[34] D. Sadek, R. Daubriac, C. Durand, R. Monflier, Q. Gravelier, A. Proietti, F. Cristiano, A. Arnoult, S.R. Plissard. Cryst. Growth Des. **22**, *8*, 5081 (2022).
[35] L. Baringthon, T.H. Dang, H. Jaffrès, N. Reyren, J.-M. George, M. Morassi, G. Patriarche, A. Lemaitre, F. Bertran, P. Fèvre. Phys. Rev. Mater. **6**, 074204 (2022).
[36] H. Okamoto. J. Phase Equilib. Diffus. **33**, *6*, 493 (2012).
[37] P. Kainzbauer, K.W. Richter, H.S. Effenberger, G. Giester, H. Ipser. J. Phase Equilibria Diffusion **40**, *4*, 462 (2019).
[38] R.N. Zitter, P.C. Watson. Phys. Rev. B **10**, *2*, 607 (1974).
[39] P. Cucka, C.S. Barrett. Acta Cryst. **15**, *9*, 865 (1962).
[40] N.A. Abdullayev, S.Sh. Kakhramanov, T.G. Kerimova, K.M. Mustafaeva, S.A. Nemov. Semiconductors **43**, *2*, 145 (2009).
[41] M.M. Otrokov, I.I. Klimovskikh, H. Bentmann, D. Estyunin, A. Zeugner, Z.S. Aliev, S. Gaß, A.U.B. Wolter, A.V. Koroleva, A.M. Shikin, M. Blanco-Rey, M. Hoffmann, I.P. Rusinov, A.Y. Vyazovskaya, S.V. Eremeev, Y.M. Koroteev, V.M. Kuznetsov, F. Freyse, J. Sánchez-Barriga, I.R. Amiraslanov, M.B. Babanly, N.T. Mamedov, N.A. Abdullayev, V.N. Zverev, A. Alfonsov, V. Kataev, B. B.chner, E.F. Schwier, S. Kumar, A. Kimura, L. Petaccia, G. Di Santo, R.C. Vidal, S. Schatz, K. Kißner, M. Ünzelmann, C.H. Min, S. Moser, T.R.F. Peixoto, F. Reinert, A. Ernst, P.M. Echenique, A. Isaeva, E.V. Chulkov. Nature **576**, *7787*, 416 (2019).

[42] I.I. Klimovskikh, M.M. Otrokov, D. Estyunin, S.V. Eremeev, S.O. Filnov, A. Koroleva, E. Shevchenko, V. Voroshnin, A.G. Rybkin, I.P. Rusinov, M. Blanco-Rey, M. Hoffmann, Z.S. Aliev, M.B. Babanly, I.R. Amiraslanov, N.A. Abdullayev, V.N. Zverev, A. Kimura, O.E. Tereshchenko, K.A. Kokh, L. Petaccia, G. Di Santo, A. Ernst, P.M. Echenique, N.T. Mamedov, A.M. Shikin, E.V. Chulkov. npj Quantum Mater. **5**, 54 (2020).
[43] N.F. Mott, E.A. Davis. Electronic Processes in Non-crystalline Materials. Oxford, Clarendon Press, (1971).
[44] T. Kurosawa, M. Matsui, W. Sasaki. J. Phys. Soc. Jpn. **42**, *5*, 1622 (1977).
[45] Y. Ootuka, A. Kawabata. Prog. Theor. Phys. Suppl. **84**, 249 (1985).
[46] C. Uher, L.M. Sander. Phys. Rev. B **27**, *2*, 1326 (1983).
[47] N.A. Abdullayev, N.M. Abdullayev, Kh.V. Aliguliyeva, T.G. Kerimova, G.S. Mehdiyev, S.A. Nemov. Semiconductors **45**, *1*, 37 (2011).
[48] N.A. Abdullayev, K.M. Jafarli, Kh.V. Aliguliyeva, L.N. Aliyeva, S.Sh. Gahramanov, S.A. Nemov. Semiconductors **51**, *7*, 942 (2017).
[49] S.I. Dorozhkin, A.A. Kapustin, S.S. Murzin. JETP Lett. **97**, *3*, 149 (2013).
[50] W.S. Boyle, A.D. Brailsford. Phys. Rev. **120**, *6*, 1943 (1960).
[51] B.I. Shklovskii, A.L. Efros. Electronic Properties of Dopped Semiconductors. Springer Series in Solid-State Sciences (1984). V. 45.

Translated by E.Ilyinskaya